Article

Characterizing Residual Current Circulation and Its Response Mechanism to Wind at a Seasonal Scale Based on High-Frequency Radar Data

Lei Ren [1,2,3], Lingna Yang [1], Guangwei Pan [1], Gang Zheng [3], Qin Zhu [4], Yaqi Wang [1], Zhenchang Zhu [4,5,*] and Michael Hartnett [6]

1   Institute of Estuarine and Coastal Research, School of Ocean Engineering and Technology,
     Sun Yat-sen University, Zhuhai 519082, China
2   Southern Marine Science and Engineering Guangdong Laboratory (Zhuhai), Zhuhai 519082, China
3   The State Key Laboratory of Satellite Ocean Environment Dynamics, Second Institute of Oceanography,
     Ministry of Natural Resources, Hangzhou 310012, China
4   Southern Marine Science and Engineering Guangdong Laboratory (Guangzhou), Guangzhou 511458, China
5   Guangdong Provincial Key Laboratory of Water Quality Improvement and Ecological Restoration for
     Watersheds, Institute of Environmental and Ecological Engineering, Guangdong University of Technology,
     Guangzhou 510006, China
6   College of Engineering & Informatics, National University of Ireland Galway, H91 TK33 Galway, Ireland
*   Correspondence: zhenchang.zhu@gdut.edu.cn

Abstract: Residual current characteristics are indicators for the net transports of sediments, nutrients, and pollutants, and for the dilution and diffusion of soluble substances in coastal areas, yet their driving mechanisms remain poorly understood. Here, we studied the characteristics of surface residual currents along the west coast of the island of Ireland, as well as the response mechanisms to wind at a seasonal scale based on the continuous observation data of high-frequency radar (HFR) for one year. Our analyses indicate that wind has a significant effect on generating surface residual currents, with correlation coefficients of 0.6–0.8 between wind speeds and residual current speeds at both annual and seasonal scales. However, the correlation between the directions of residual currents and the wind was not as significant as speed, likely because the directions of residual currents were not only affected by sea surface wind, but also by land boundary conditions in the research area. Moreover, the residual currents had a significant eastward flow trend identical to the wind direction at the maximum wind speed time, during which the effect of the tide on residual currents was relatively weak. Additionally, when compared with wind fields, HFR surface flow fields and surface residual current fields show that wind is the dominant driver of the variations of surface and residual flow fields. These findings shed light on coastal ecological and environmental management and can assist in the prevention and mitigation of marine disasters, by providing helpful information for improving the ability and accuracy of forecasting coastal currents.

Keywords: high-frequency radar; residual currents; wind speed; surface flow field; seasonal scale

1. Introduction

To meet economic development needs, human beings use marine space to carry out construction, such as offshore airports, offshore sightseeing platforms, offshore construction platforms, island reef construction, and so on [1]. The offshore engineering and structures not only meet their own design functions but also bear various complex and severe ocean loads, including ocean currents. The stability of marine engineering and structures under ocean currents are complex dynamic response processes. Investigations into the driving mechanisms of ocean currents are not only important scientific issues but also key practical issues to be solved in marine disaster prevention and mitigation.

Ocean currents are important parameters used to describe the movement of seawater. Others can be classified as residual currents, except for periodical tidal currents. Residual currents refer to the remaining parts of the total ocean currents after deducting periodic currents. The movements of residual currents are unidirectional (different from the periodic tidal currents). Thus, residual currents can move for long distances in certain directions [2]. Although the magnitudes of residual currents are not large, they are directly relative to the directions of sediment movements, the net transports of nutrients and pollutants, and the dilution and diffusion of soluble substances [3]. An analysis of residual currents is also an effective method to study coastal sediment movement and environmental protection engineering [4]. By analyzing the response of residual currents to wind in the study area, the diffusion of industrial wastewater, domestic wastewater, and ship oil spills in seawater can be prevented and reasonably treated [5].

Studies have adopted different methods to analyze residual currents, depending on the data sources; for instance, the veering angles of wind-driven currents within the surface layer range from 0° to 45° to the right of the wind direction (northern hemisphere), and its magnitudes are 2–3% of the wind speed. Thus, a wind map was introduced to present the fractional variance of surface currents by Kim et al. [6]. Moreover, the transfer functions in the summer and winter are presented, which were used to examine the seasonal variations in ocean surface current responses to the wind. Because Eddy-topography interactions (topographic stress) are difficult to resolve with numerical models, a parameterization was proposed by Holloway [7] based on the statistical mechanical equilibria tendencies (Neptune effect). Most of the studies mentioned above focused on the long-term behaviors of ocean currents, which were based on monthly or even seasonal mean data. By contrast, Callies et al. [8] used daily meteorological data and current data for the principal component analysis to assess changes in the North Sea circulation.

Residual currents can be affected by many factors, including topography, wind field, runoff, non-linear factors of inshore tidal waves, uneven seawater density, sea surface tilt, and other factors [9,10]. Previous studies found that the residual current circulation dynamic process is significantly affected by sea–air coupling [11]. Wind transfers energy into the ocean through a multi-scale ocean motion, which is the main source of mechanical energy driving mixing in oceans [12]. Due to the consumption of momentum by viscous forces in seawater movement, the wind has the greatest influence on surface currents, and weakens with the increase of water depth. Since the wind acts directly on the upper layers of the water column, residual currents generated by the wind are predominated by surface processes. However, whether (and how) residual currents correlate with wind remains poorly understood.

In this study, we investigated the characteristics of surface residual currents along the west coast of the island of Ireland and the response mechanisms to wind at a seasonal scale, based on the continuous observation data of high-frequency radar (HEF). HFR has been widely used to monitor surface currents for coastal areas around the world [13]. Specifically, we used current data based on HFR and Butterworth filters to obtain residual surface currents and, subsequently, variations in residual currents. We combined such data with the wind field data to analyze the driving effects of the wind on residual currents at a seasonal scale, as winds in the study area are relatively large and have significant seasonal characteristics [14].

The outline of this paper is as follows. Section 2 presents a brief description of the methodologies used in this study, HFR system, atmospheric data, and computations of residual surface currents. Section 3 presents the results of residual surface currents to wind and the influence of the wind on residual currents, followed by a discussion in Section 4. Section 5 presents the main conclusions.

2. Methodologies

2.1. Study Area

The study area is located on the west coast of the island of Ireland, as shown in Figure 1. This area has westerly winds and ocean current movements that are strongly affected by the North Atlantic Oscillation and frequent low-pressure systems [15,16]. The bathymetry in the study area ranges from 0 to 140 m, and the nearshore isobaths are roughly parallel to the coastlines. The average wind speeds (affected by the Atlantic meteorological system) in January and June are approximately 11 m/s and 7 m/s, respectively [17]. This Atlantic wind condition has a significantly important impact on the size and direction of the local residual current in the region, and the surface residual current is controlled by wind forcing. Previous studies on hydrodynamic characteristics in this area are mainly based on numerical modeling; observations over a large domain with fine temporal and spatial resolutions were rarely obtained and used. This is the first time that surface currents were continuously monitored and residual currents were extracted in this area [18,19].
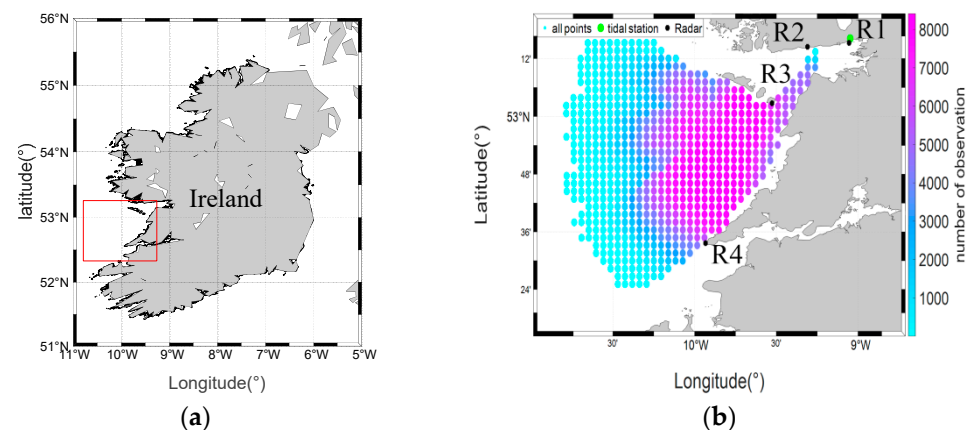

Figure 1. Study area and HFR coverage. (**a**) location of study area; (**b**) HFR coverage area and radar sites (R1–R4 indicate the four HFR sites in the study area, respectively).

Western Ireland has some of the highest resources of wind and wave energy in the world. In April 2021, the Irish National Electricity Supply Board (ESB) announced a detailed plan to immediately start the development of a 1.4 GW offshore floating wind farm in this region, which will be one of the largest marine renewable energy projects in the world. After completion, Ireland will become an exporter of clean energy. This will provide great social contributions to Ireland and Europe. Thus, research into the hydrodynamics of this area will be of great importance for the planning, construction, and operation stages of this project.

The deployment locations of HFR stations and the coverage areas are shown in Figure 1b. This study focuses on the analysis of sea surface currents observed by the HFR system from a year's worth of data, covering the offshore area with the maximum meridional and latitudinal lengths of approximately 100 and 90 km, respectively (see Figure 1b). To ensure the reliability and integrity of the analyzed dataset, sea surface currents monitored for more than 80% of the observation period are defined as high-density points; in total, 162 points (see Figure 1b). Surface currents at these points were selected for the following analysis. The maximum latitudinal length and meridional length of high-density monitoring areas were approximately 40 and 50 km, respectively. Figure 1b shows that the majority of the high-density points were distributed at the intersection area between two HFR stations.

Wind data from an atmospheric model were provided by the European Centre for Medium-Range Weather Forecasts (ECMWF, https://www.ecmwf.int/ (accessed on 1 December 2015 to 31 December 2016). Detailed descriptions of each dataset are presented next.

2.2. HFR System

HFR is an advanced type of remote sensing observation equipment that has the advantages of large horizons, wide ranges, and all-weather conditions [20]. HFR can extract sea state information, such as wind field, wave field, and flow field from radar echo [21,22]. Take the flow field, for example. Its observation principle is based on Bragg scattering [23]. The electromagnetic wave with wavelength λ emitted by HFR is incident of the ocean surface and propagates along the ocean surface. When encountering the ocean surface wave with wavelength λ/2 and the propagation direction of the wave toward or away from HFR, the backscattering is the strongest, which is called Bragg scattering [24]. According to this principle, the echo spectrum can be obtained. The wave propagating toward the radar produces a positive spectrum peak, while the wave propagating away from the radar produces a negative spectrum peak [25]. This phenomenon is called the Doppler frequency shift. In the case of surface current, the echo spectrum will generate a small frequency shift on the basis of the standard Doppler frequency shift. The radial current velocity in the detection area can be obtained by inversing the small frequency shift through the corresponding relationship between the currents and the echo spectrum. The flow field data in the observation area can be obtained by superimposing the radial flow data measured by two or more HFR stations [15,26,27].

Since Crombie discovered Bragg scattering in 1955, research into HFR has been carried out rapidly (based on it). After several research and development stages, it has been widely used in ocean remote sensing observations [28]. At present, the retrieval algorithm of current velocity detected by HFR is relatively mature, can obtain high-precision long-time series current data, and is suitable for the analysis of marine dynamic processes [29].

In this study, data were obtained from four HFR stations deployed by the National University of Ireland, Galway. In 2011, the portable Seasonde HFR stations R1 and R2 produced by Coastal Ocean Dynamics Application Radar (CODAR) company were deployed. Their operating frequencies were 26.425 and 24.64 MHz, respectively; their transmitted bandwidth was 499.88 KHz, range space was 0.3 km, velocity threshold was 150 cm/s, temporal resolution was 60 min, and data-averaging period was 94 min. The accuracies of HFR data were obtained by comparing the sea surface flow observed by the HFR monitoring network of the R1 and R2 stations with ADCP (Acoustic Doppler Current Profiler) data in the same region. The value of the root mean square error (RMSE) was 10–12 cm/s, which proved the reliability of HFR observation data [30]. In 2014, two other HFR stations, R3 and R4, were added to the west coast offshore area, and four stations were connected after that. The operating frequency of R3 and R4 was 13.5 MHz, the transmitted bandwidth was 49.63 KHz, the range space was 3 km, the temporal resolution was 60 min, and the data averaging period was 75 min. Surface currents over a depth of approximately 1 m from December 2015 to December 2016 monitored by the HFR system were selected and used in this study. The HFR processing system preliminarily controls the data quality, and the maximum current speed is set at 150 cm/s.

2.3. Atmospheric Data

Since coastal surface currents are sensitive to wind conditions, to further investigate the relationship between wind and residual currents, wind data obtained from the European Centre for Medium-Range Weather Forecasts (ECMWF) at $0.125° \times 0.125°$ spatial resolution with 6 hours' temporal resolution were used.

To study wind variation characteristics during the analysis year, a wind rose (of ECMWF data) for 2016 is shown in Figure 2. In general, wind direction refers to the direction in which the wind blows from, and the direction of residual currents refers to the directions in which the residual currents flow to. In the subsequent rose diagram, the wind direction and the residual flow direction are plotted based on the same definition.
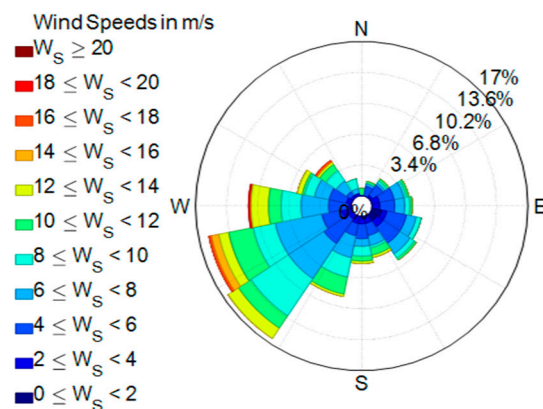
Figure 2. The wind rose for the full year (2016).

The variation in the range of wind speeds was from 0.03 to 21.96 m/s. The average wind speed was 7.28 m/s. Its dominant wind direction was southwest, accounting for approximately 40% of the whole year; while winds from the northwest direction accounted for nearly one-third of the whole year, indicating that the wind direction in the study area was mainly western, which is consistent with the fact that study area is located in the westerly belt [16].

2.4. Extraction of Residual Surface Currents

In order to extract residual current data, a filtering technique is commonly used in physical oceanography to smooth and extract the time series, remove the fluctuation in the selected frequency band, and change the signal phase. In this study, high-frequency oscillation signals need to be filtered from the original HFR dataset.

There are a number of filters used in physical oceanography analysis such as Running-mean filters, Lanczos-window cosine filters, Kaiser-Bessel filters, and Butterworth filters. Running-mean filters are the simplest but their frequency responses are poor in a relatively short dataset. Other filters mentioned above are more complex and precise. Lanczos-window cosine filters are simple and the filtering effect is better due to that the Lanczos window can reduce the leakage of redundant signals to the passband. When the filter parameter *n* is large enough, the Lanczos-window cosine filter has a better ability to filter out the required information and suppress the interference information [31]. The Kaiser-Bessel filter is one of the best filters to process ocean data. It requires the specification of a single parameter, and easy to generate coefficients with high equivalent noise bandwidth. Butterworth filters were used in this research considering the filtering effect and proficiency. This is a special type of recursive filter. Its transfer function is created by using rational functions in sine and cosine, and its output consists of input data and output past values. Different from the transfer function of the linear non-recursive filter constructed by truncated Fourier series, the transfer function of the Butterworth filter is monotonically flat in the pass band and stop band, and has high tangency at the origin and Nyquist frequency [32]. Thus, the Butterworth filter was selected and applied to extract residual surface currents.

In this research, raw surface current data from a HFR system were filtered using the second-order Butterworth filter. The high-frequency signals (mainly the semidiurnal tide periodic signal represented by M2 and S2 tides) were filtered out, and the non-periodic characteristics (residual currents) contained in the raw data were retained. Through the comparison of filter threshold settings and filtering effects, the threshold value of the second-order Butterworth filter was set to 33 h, filtering out the semidiurnal and diurnal tide signals from raw HFR surface currents, and retaining the low-frequency residual

currents signal [33]. The second-order transfer function of the Butterworth low-pass filter can be expressed in the following formula [34]:

$$|H(\omega)|^2 = \frac{1}{1+\left(\frac{\omega}{\omega_C}\right)^{2n}} = \frac{1}{1+\varepsilon^2} \times \frac{1}{\left(\frac{\omega}{\omega_p}\right)^{2n}} \tag{1}$$

where n is the order of Butterworth low-pass filter, ω_C is the cut-off frequency, ω_p is the edge frequency, and $\frac{1}{(1+\varepsilon^2)}$ is the passband edge value of the low-pass filter. In the research, values of ω_C and ω_p were set as 11.88 kHz and 3.6 kHz respectively in this research based on application by Mihanović et al. [35].

3. Results

3.1. Response of Residual Surface Currents to Wind

To study the relationship between wind and residual surface currents, statistics of ECMWF wind speeds and HFR residual currents during the full analysis year and four seasons are computed and presented in Table 1.

Table 1. Statistics of wind speeds and HFR residual surface vector speeds.

Variable	Statistics	Spring (March–May)	Summer (June–August)	Autumn (September–November)	Winter (December–February)	Full Year
Wind Speed (m/s)	Maximum	21.31	14.28	18.26	21.96	21.96
	Average	6.64	6.38	7.21	9.03	7.28
	Minimum	0.14	0.13	0.03	0.42	0.03
Residual Current Speed (cm/s)	Maximum	25.12	27.17	35.65	41.18	41.18
	Average	10.12	9.86	12.36	16.28	11.8
	Minimum	0.63	0.2	0.25	0.31	0.16

Both wind speed and residual current velocity display clear seasonal variation (Table 1). The maximum annual wind speed of 21.96 m/s and the maximum residual current velocity of 41.18 cm/s occur in the winter. In addition, the average wind speed (9.03 m/s) and averaged residual current velocity (16.28 cm/s) are the largest in the winter. The average wind speed and residual current velocity are least in the summer; while the maximum residual current velocity in spring is a minimum.

To explore the response mechanisms of residual surface currents to wind, the rose diagram and vector diagrams of spatially-averaged residual surface current vectors and wind vectors over the full analysis year are shown in Figures 3 and 4, respectively.
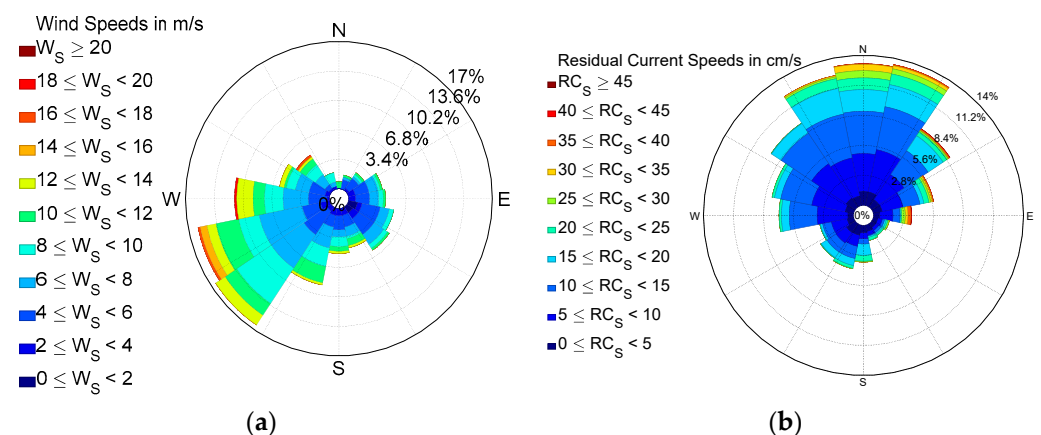

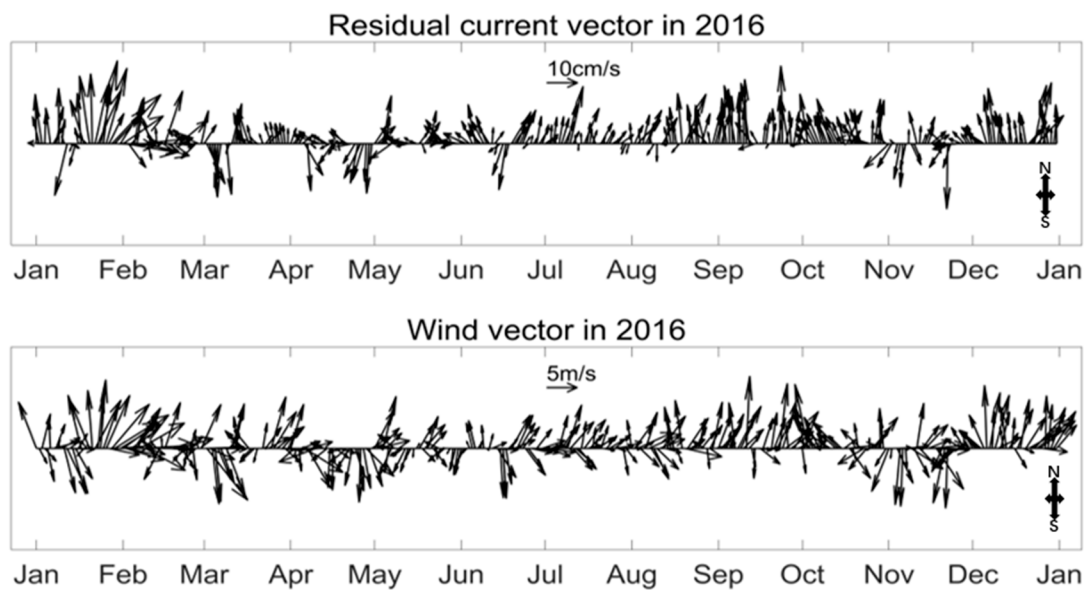**Figure 3.** Rose diagrams for the full year (2016) (**a**) wind; (**b**) residual currents.

Figure 4. Vector time series of residual currents and winds during the analysis.

Wind speed is between 0 and 22 m/s during the analysis period in the study area, and the residual current velocity magnitude is between 0 and 42 cm/s. The dominant wind direction is southwest, accounting for approximately 40% of the whole analysis year; while the northwest wind direction accounts for approximately one-third. This indicates that the wind is mainly westerly during the analysis period, this is consistent with the geographic location of the study area. From the statistical analysis, correlation coefficients of zonal and meridional components between wind vectors and residual currents vectors over the analysis year are 0.76 and 0.68, respectively. This further indicates that residual surface currents in the study area are significantly affected by wind.

To further explore the influence of the wind on coastal surface residual currents in different seasons, detailed correlation analyses between wind and residual currents in four seasons were carried out as detailed below.

Wind speed in spring is between 0 and 22 m/s, and the residual current velocity is between 0 and 26 cm/s. Figure 5 shows that the direction of residual currents is mainly west and northwest. While there is no obvious wind direction in the spring rose diagram in the wind directions, the directions of east and southwest take the larger proportions. Correlation coefficients of zonal and meridional components between wind speeds and residual currents speeds are 0.74 and 0.70, respectively. This indicates that wind is the main driving force generating residual surface currents. However, the directions of residual currents do not correlate well with the directions of the wind. Because the study area is a coastal region with a small scale (40 km × 50 km), though the movements of residual currents are driven by wind force significantly according to the relative analysis, the residual current directions are also influenced by the land mass in the study area. As shown in Figures 5a and 6 the southerly wind is significant in spring. The southerly winds 'render' the residual currents varying into westerly directions due to the block of land of the west coast. This explains the difference between directions of wind and residual currents in Figures 5 and 6. The vector time series in Figure 6 shows that the direction of residual currents has good agreement with the wind direction in spring according to the correlation analysis. Only in the middle of April and the middle of May, the residual current vector shows a trend in the northwest direction, while the wind vector shows a trend of southerly wind. This may be due to the effect of topography variation in a small scale (40 km × 50 km) region [36].
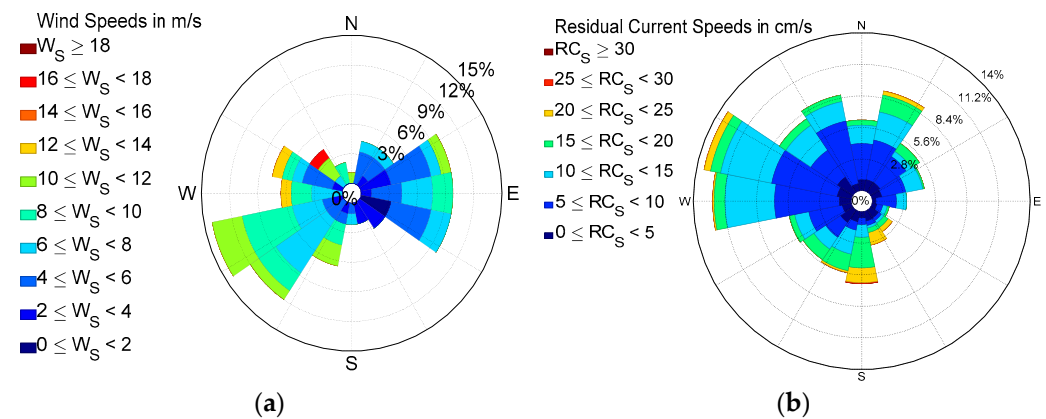
Figure 5. Rose diagram during spring. (**a**) wind; (**b**) residual currents.
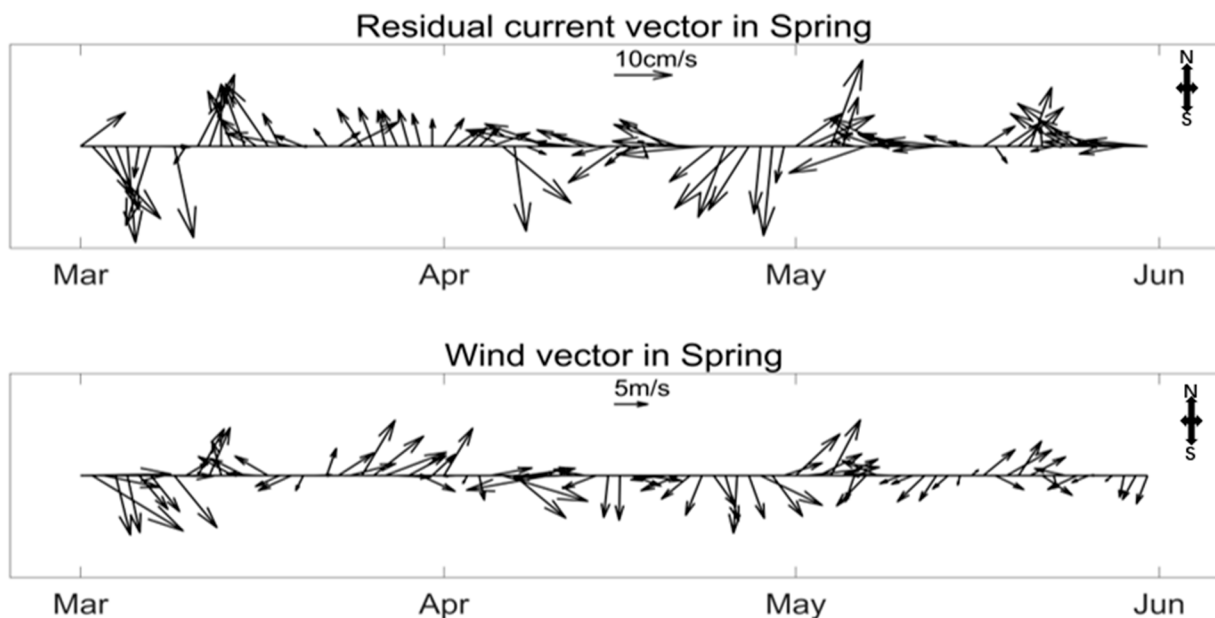

Figure 6. Vector time series of residual currents and winds in spring.

From Table 1, the average wind speed in the summer is 6.38 m/s and the maximum wind speed in the summer is 14.28 m/s, which are the minimum values in the statistics for four seasons and the full year. As is shown in Figure 7, the main residual currents' direction is northeast while the wind direction is southwest. The direction of wind and residual currents qualitatively compare well. However, the difference between the direction of the residual currents and the wind direction can be shown in the summer vector diagram, as shown in Figure 8. The average wind speed, the maximum wind speed, and the average and maximum velocity of residual currents are the lowest of the four seasons. A good agreement exists between wind vectors and residual surface vectors when the wind speed is high, see Figure 8. Correlation coefficients of zonal and meridional components between residual currents vectors and wind vectors are lower in the summer than in other seasons at 0.69 and 0.61, respectively. It shows that the direction of residual flows in the summer had a significant difference when wind speeds are low. Fernand, Nolan, Raine, Chambers, Dye, White, and Brown [17] indicated that currents speed and direction did not correlate well except during the period with strong south-westerly winds. Therefore, the current directions are not only driven by wind but also affected by the topography in the study area.
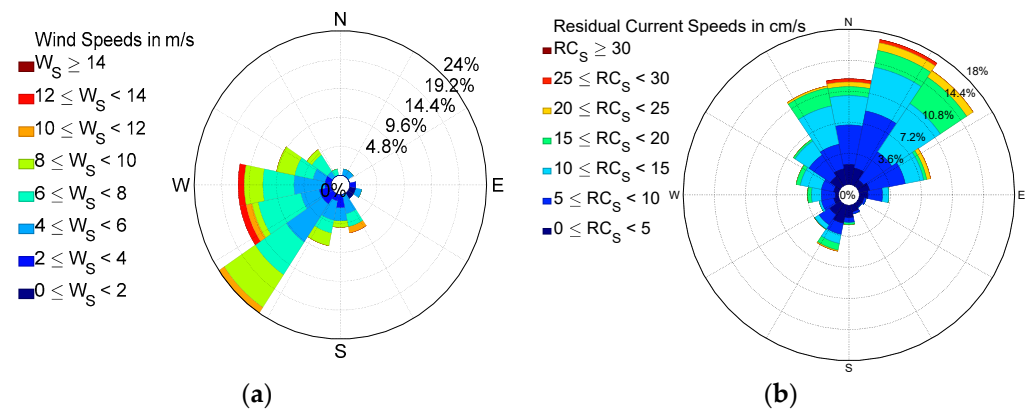
Figure 7. Rose diagram for summer. (**a**) wind; (**b**) residual currents.
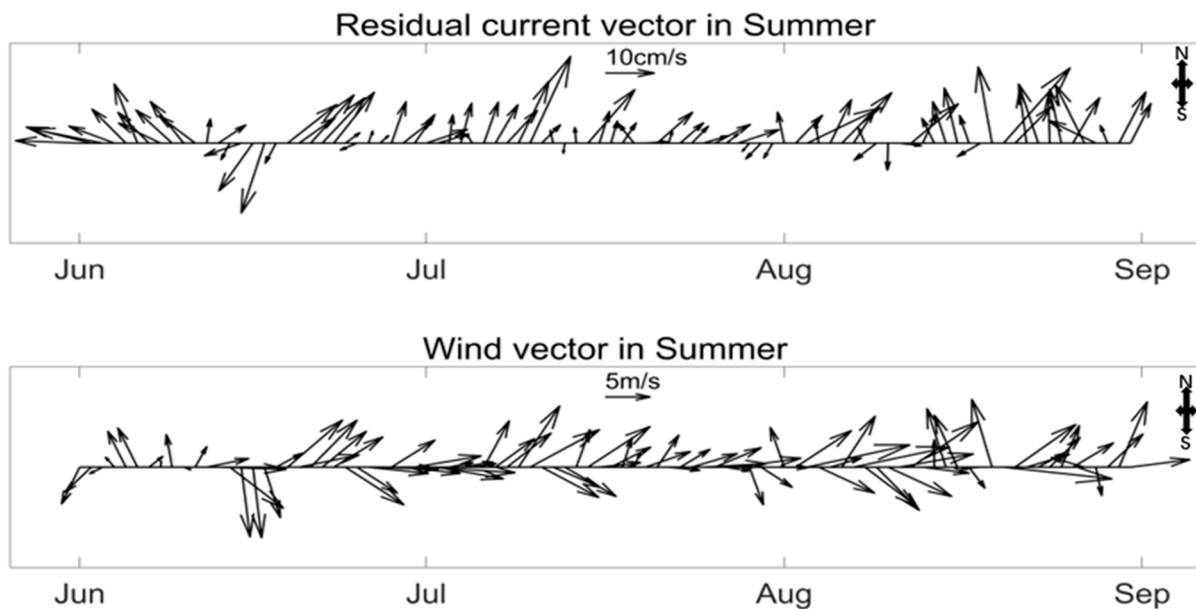

Figure 8. Vector time series of residual currents and winds in the summer.

Wind speed in autumn is between 0 and 19 m/s, and the residual current velocity is between 0 and 36 cm/s. Averaged residual currents' velocity, the maximum residual currents' velocity, averaged wind speed and maximum wind speed of other currents are only lower than in the winter. The direction of residual current flow in autumn is mainly from south to north, as is shown in Figure 9. Wind direction distribution in autumn is diverse, but southwest is still the dominant direction, followed by southeast. The correlation between wind speed and residual current velocity in autumn is the highest, as is shown in Figure 10. Correlation coefficients of zonal and meridional components between residual currents vectors and wind vectors are 0.8 and 0.75, respectively. Statistically good agreement between wind direction and residual currents direction existed in autumn. This indicates that wind has a significant impact on driving residual current flow in autumn.
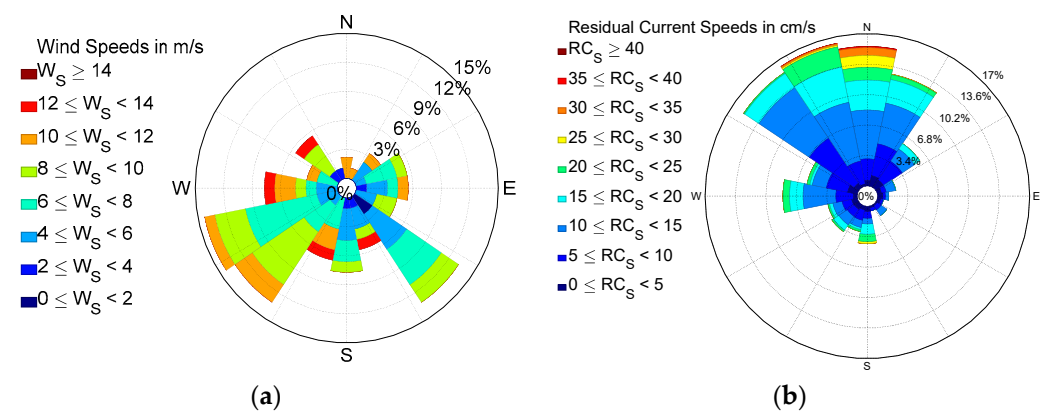
Figure 9. Rose diagram for autumn. (**a**) wind; (**b**) residual currents.
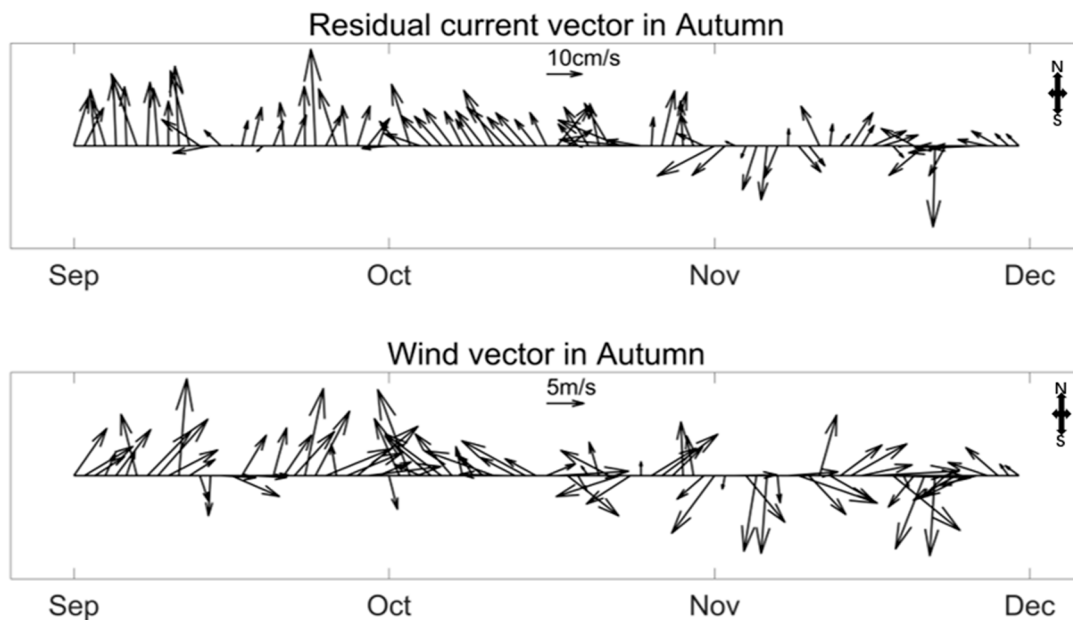

Figure 10. Vector time series of residual currents and winds in autumn.

In the winter, the wind speeds are between 0 and 22 m/s, the maximum wind speed occurs in this season; the residual currents velocities are between 0 and 42 cm/s, and the maximum residual current velocity occurs in this season. Figure 11 shows that the dominant flow direction in the winter is northeast, followed by northwest. The northern flow trend is significant. The correlation coefficient of zonal and meridional components between residual currents vectors and wind vectors are 0.75 and 0.6, respectively. Figure 12 showed that the direction of residual currents had a strong response to wind direction variation in the winter except for the first ten days in February when a northwest wind occurred.
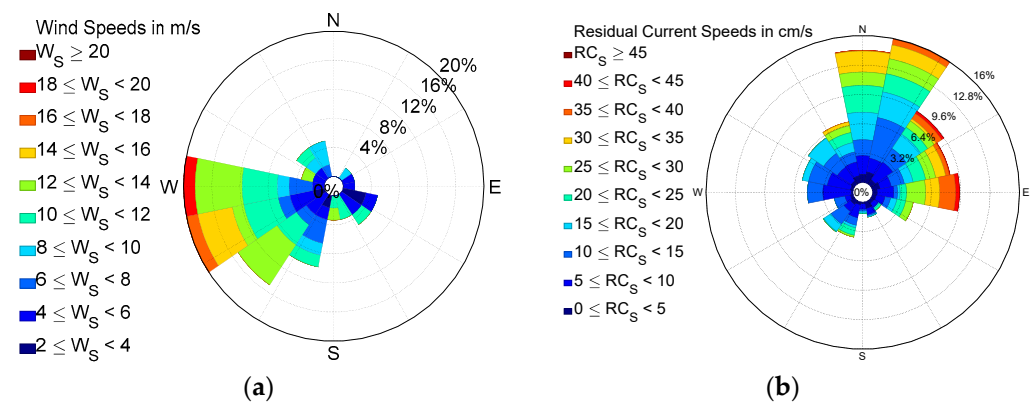
Figure 11. Rose diagram for winter. (**a**) wind; (**b**) residual currents.
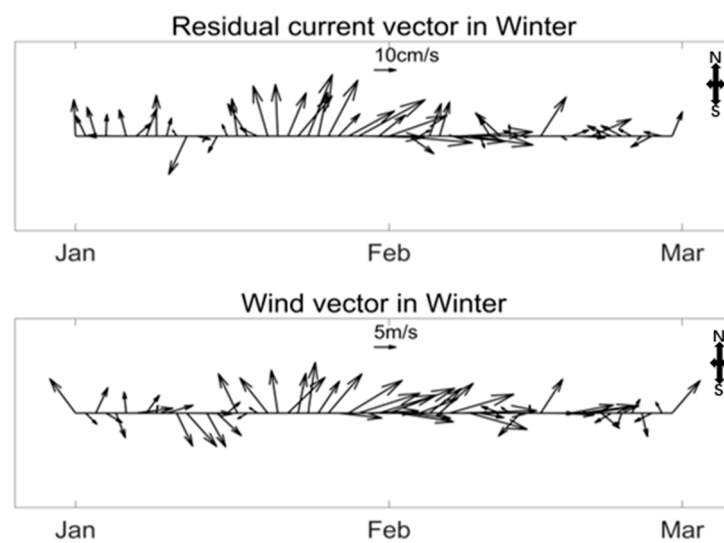

Figure 12. Vector time series of residual currents and winds in the winter.

3.2. Influence of the Maximum Wind on Residual Currents

To investigate the influence of regional wind fields on surface residual flow fields under extreme wind speed conditions at a seasonal scale, wind vector fields, current vector fields, and residual current vector fields corresponding to the maximum spatially-averaged wind speed (21.31 m/s, 14.28 m/s, 18.26 m/s, 21.96 m/s, see Figure 13) in the four seasons are analyzed. Through comparisons between wind fields and residual current fields at the time of the maximum wind speed during the four seasons, the effect of wind stress on the movement of residual currents is significant. At the moments corresponding to maximum spatially-averaged wind speeds, residual current velocity is high; the strength of the wind field and the residual current vector field have a high correlation.

Figure 13 shows that the maximum wind speed in spring occurs in an ebbing tide, and the dominant wind direction is northwest (shore wind). At this time, the residual current field presents an onshore flow tendency, which is not affected by the tidal force at this time. This reflects that the main driving factor of residual currents is wind stress, and tidal signals are well filtered after using the second-order Butterworth method. At this time, the directions of the current field and the residual current field correlate well, showing a significant trend of onshore flow tendency, deeply affected by the wind stress and not reflecting the characteristics of the flow pattern in the ebb tide period.
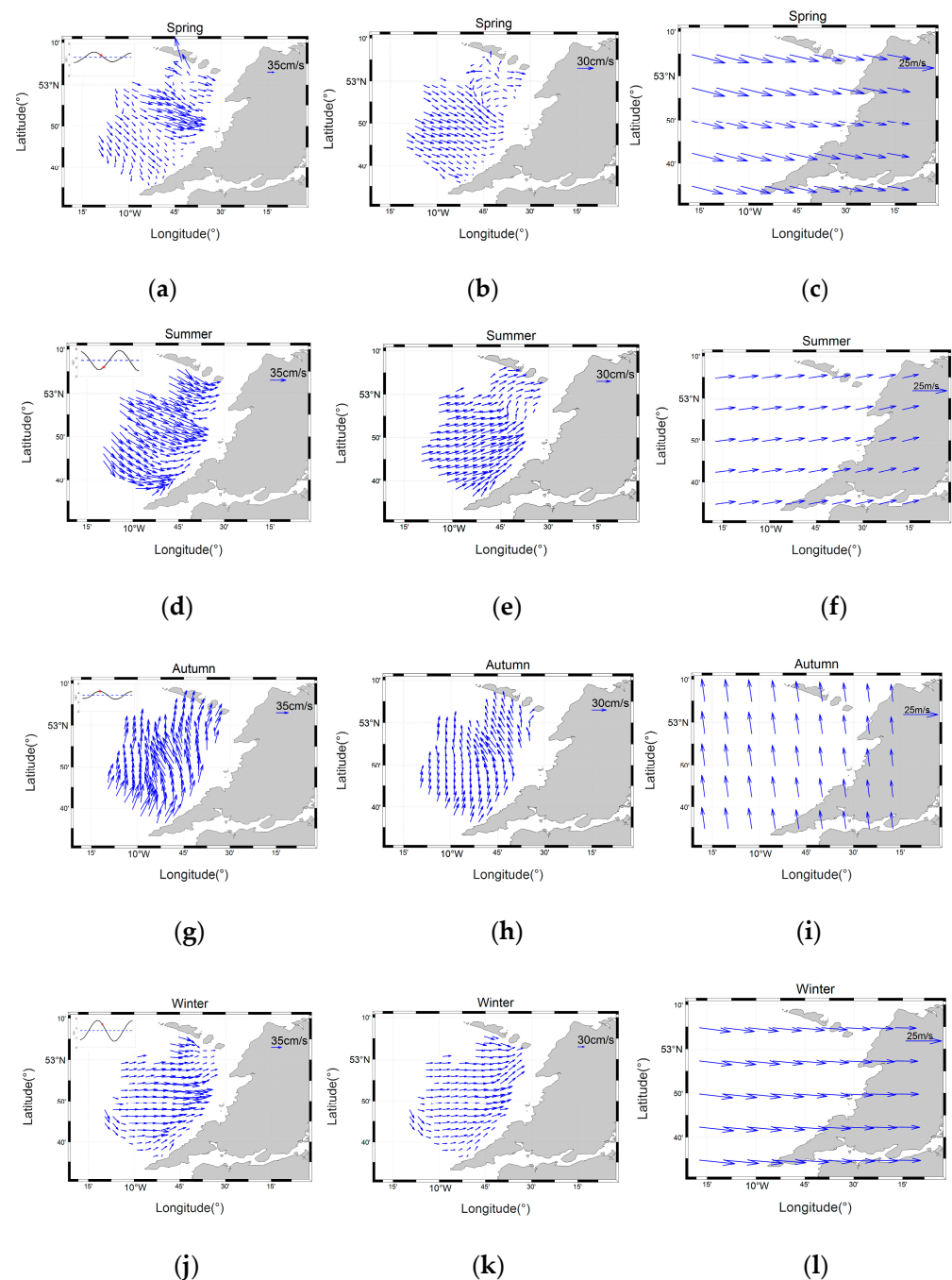
Figure 13. Residual surface current vectors and HFR current vector fields corresponding to the maximum atmospheric wind fields during four seasons. (**a**,**d**,**g**,**j**) are original currents from HFR; (**b**,**e**,**h**,**k**) are residual currents; (**c**,**f**,**i**,**l**) are wind vectors. The panels at the top left of (**a**,**d**,**g**,**j**) are the tidal phrase corresponding to the maximum wind time (the red dot in the top left subfigure is the tide level at the corresponding analysis time).

The maximum wind speed in the summer is during a rising tide, and the dominant wind direction is southwest, consistent with the direction of tidal dynamics. The residual flow exhibits a strong onshore flow characteristic. At the same time, the dominant flow direction of the current field is different from that of the residual current field in the same period at some spatial points, but its trend is consistent overall, which shows the characteristics of onshore flow.

The maximum wind speed in autumn is at slack flood tide. The direction of the residual currents is mainly affected by a southerly wind, which exhibits a northward flow

tendency. Onshore flows are not obviously presented during this period. The currents direction is consistent with that of the residual currents, showing a trend of northward flow.

In the winter, the maximum wind speed is during an ebbing tide. The wind direction is westerly, which is uncorrelated with the direction of tidal dynamic propagation.

There is a significant correlation between the spatially-averaged residual current vector direction and the spatially-averaged wind vector direction at the time of the maximum wind speeds. The corresponding relationship between the wind direction and the direction of residual currents from spring to autumn can be seen directly. For the maximum wind speed in the winter, the wind direction and direction of residual currents present obvious characteristics of westerly and easterly, the movement of the residual currents and wind is mainly in the zonal velocity component, and their movement in the meridional velocity component is not obvious; therefore, the residual current vector and wind vector at the maximum wind speed point in the winter still correlates well.

The wind speed range, as presented in Table 2, was from 12.12 m/s to 27.1 m/s at the time of the maximum wind speed in each season, the range of residual current vectors was from 1.85 cm/s to 73.26 cm/s, and instantaneous surface current speed range of HFR was 3.95 cm/s to 100.24 cm/s. At four times the maximum wind speed, the average speed of the current observed by HFR was greater than the corresponding residual current speed. Among them, the average value of the current velocity was 25% larger than that of the residual current velocity. The range of the current values measured by HFR was 34.84% larger than the range of residual current values; the range of the current value was 96.29 cm/s and that of residual current was 71.41 cm/s. The range and magnitude of the residual current velocity being smaller than those measured by HFR prove that the tide filtering process in this study is effective. Table 2 further shows that the residual current vector and current vector at the time of the maximum wind speed were mainly driven by wind stress.

Table 2. Statistics of the maximum wind for each season.

Variable	Statistics	Spring	Summer	Autumn	Winter
Wind Speed (m/s)	Maximum	25.68	16.05	21.19	27.1
	Minimum	15.17	12.12	14.74	13.73
	Average	21.32	14.32	18.26	21.98
Residual Surface Current Speed (cm/s)	Maximum	22.26	36.82	38.83	73.26
	Minimum	1.85	9.19	13.71	12.97
	Average	13.73	23.84	23.73	38.64
Surface Current Speed (cm/s)	Maximum	66.65	41.44	62.89	100.24
	Minimum	3.95	8.5	22.85	10.65
	Average	20.21	23.85	40.42	40.49

The dominant wind direction of the spatial wind field during the spring maximum wind speed is northwest, and the corresponding residual currents flow field's direction is northwest in the majority of the study area and east in the area near the island in the north. The residual currents direction in most of the study area shows southeast flows corresponding to the northwest wind.

The dominant wind direction of the wind field corresponding to the maximum spatially-averaged wind speed in the summer is southwest, while the residual current field shows a trend in the northeast direction. The difference in the distribution of the residual currents in the northern parts of the study area is due to the blocking of the northern islands, which shows a trend of northern flow.

The dominant wind direction of the wind field at the time point corresponding to the maximum spatially-averaged wind speed in autumn is south, while the residual current field shows a trend of northward flow. The residual current field corresponding to the maximum wind speed in autumn is different in the southern and northern parts of the

study area. The residual currents in the northern part of the study area are blocked by the northern island, showing a trend of flow to the northwest, while the residual currents in the southern part of the study area show an obvious northward flow trend.

The dominant wind direction of the wind field at the time point corresponding to the maximum spatially-averaged wind speed in the winter is westerly, while the residual currents in the northeast sea area show the trend of northeast flow, the residual currents in the southwest sea area show the trend of southeast flow, and the residual currents in other sea areas show the trend of east flow.

In conclusion, the wind fields and the residual current vector fields corresponding to the maximum averaged wind speed in four different seasons exhibit a significant spatial consistency.

4. Discussion

In this research, the HFR surface currents over a continuous year are divided into four groups at a seasonal scale to discuss the response of surface residual currents to wind. Daily averaged wind vectors and residual currents vectors are compared for each analysis season. The same time series were used to compute correlation coefficients, but the hysteresis of the residual current response to the wind is not considered. Xing et al. [37] found that the lag of the residual current response to the wind varies from several hours to more than ten hours. In the analysis at a daily scale, it is possible to further improve the correlation between residual currents and wind by deeply analyzing the influence of the lag effect.

The veering angles of the wind-induced residual currents range from 0 to 45 degrees to the right of the wind direction in the northern hemisphere [6]. Because the study area is located in the coastal area, the effects of topography and shoreline cannot be ignored. The angle between $-90°$ and $90°$ can be considered, i.e., the residual currents are caused by the wind [10]. When discussing the drifting in the finite deep sea, except that it is necessary to introduce a hypothesis of limited depth, the other assumptions are the same as those in the infinite deep sea, the solution satisfying the boundary conditions can be expressed as [31]:

$$W = \frac{(1+i)\tau_y}{2a A_i \rho} \frac{\text{sh}(1+i)a\xi}{\text{ch}(1+i)ah}$$ (2)

where complex velocity $W = u + iv$, complex press $\tau = \tau_z + i\tau_y$. It can be seen that the smaller the water depth, the smaller the right deflection angle of the velocity with the increase of depth. In the ocean with very shallow water depth, the drifting flows almost along the wind direction from the surface to the seabed. Considering the influence of topography and water depth, the residual flow driven by wind can be distinguished more accurately. Moreover, the corresponding relationship between wind speed and residual currents in the study area can be further improved.

Residual currents include tidal residual currents, wind ocean currents and density currents. The wind force in the study area is strong, but the effect of tidal currents cannot be ignored. When a tidal wave is transmitted from the ocean to nearshore, non-linear effects are enhanced due to the shallower water depth, and tide-induced residual currents will be generated [38]. In the follow-up research, researchers can further study the response of residual currents to the wind during both spring and neap tides. In the neap tide period, there may be a stronger correlation between residual currents and the wind, which will further advance the study of wind mechanisms of the wind on residual currents. Although residual currents are mainly driven by wind forces in the study area, the direction of the residual currents is also influenced by the topography, especially during the periods of low wind speeds. In order to study its profound mechanisms, analysis of the residual water level can be exerted to figure out how the topography of the study area makes a deflection between wind directions and residual current directions through the difference of barotropic gradient made by the sea level fluctuation in further study. The prediction of currents in the study area will be exerted in further studies using machine learning methods. Through the analysis of the mechanism of currents in the study area, the vital

driven factors of the currents will be chosen as the input of the prediction model and will implement the prediction of currents in the study area.

Additionally, hydrodynamics is an important power source for material transport in coastal areas, and suspended sediment transport is an important embodiment of the hydrodynamic change process. Residual currents are a special non-periodic form of ocean current. Its variation characteristics indicate the net transport and long-term transport of estuarine and coastal materials, and the change of residual current structure makes the mechanism of suspended sediment transport quite different on different temporal and spatial scales. Therefore, the investigation into characteristics of residual current circulation and the response mechanisms to wind at a seasonal scale is of great importance for exploring material transport in the study area.

5. Conclusions

The analysis of characteristics of residual surface currents on the west coast of the island of Ireland was carried out based on one-year continuous observations monitored by the HFR system. The main conclusions are as follows.

(1) The correlation coefficient of the annual and seasonal wind speeds and surface residual current velocity was 0.6–0.8, showing a relatively strong correlation between the wind and residual surface currents.

(2) From the direction of the residual current field and the corresponding wind rose diagram, the correlation between the direction of residual currents and the wind direction was not as significant as speeds, likely because the direction of residual currents was not only affected by sea surface wind, but also by land boundary conditions in the research area.

(3) The residual currents were affected by wind stress, presented characteristics of an eastward flow, and did not show the characteristics of onshore flow corresponding to the period of the flood tide. At the time corresponding to the maximum wind speeds in four seasons, the tidal force did not show significant effects on the distribution of currents and residual current directions. The surface currents and residual currents were mainly affected by wind force instead. At times of the maximum wind speed, wind stress was the main driving factor for both the residual flow field and current field.

In short, the investigation into the response of residual surface currents to wind was undertaken based on observations from the HFR system on the west of the island of Ireland. These findings are useful for ecological environment protection and treatment. The correlation between wind and residual surface currents provides important information for developing soft-computing forecasting models based on artificial intelligence, which will be carried out in future research.

Author Contributions: Formal analysis, G.P., L.Y., Z.Z., Y.W. and L.R.; investigation, writing—original draft preparation, G.P., L.Y., G.Z., Z.Z. and L.R.; writing—review and editing, L.R., M.H.; visualization, Q.Z., Y.W. and G.P.; supervision, M.H., L.R.; funding acquisition, Z.Z., M.H. and L.R. All authors have read and agreed to the published version of the manuscript.

Conflicts of Interest: The authors declare no conflict of interest.

References

1. Kim, S.J.; Kõrgersaar, M.; Ahmadi, N.; Taimuri, G.; Kujala, P.; Hirdaris, S. The influence of fluid structure interaction modelling on the dynamic response of ships subject to collision and grounding. *Mar. Struct.* **2021**, *75*, 102875. [CrossRef]
2. Wang, B.; Hirose, N.; Moon, J.-H.; Yuan, D. Difference between the Lagrangian trajectories and Eulerian residual velocity fields in the southwestern Yellow Sea. *Ocean Dyn.* **2013**, *63*, 565–576. [CrossRef]

3. Shi, M.C. *Physical Oceanography*; Shandong Education Press: Jinan, China, 2005; Volume 60–120.
4. Yang, J.; Ding, W.; Cui, J.; Guo, S.; Iop. Characteristical analysis of tidal and residual currents in the sea area around Tangshan international tourism island. In Proceedings of the Asia Conference on Geological Research and Environmental Technology (GRET), Electr Network, Kamakura City, Japan, 10–11 October 2020. [CrossRef]
5. Liu, G.; Liu, Z.; Gao, H.; Gao, Z.; Feng, S. Simulation of the Lagrangian tide-induced residual velocity in a tide-dominated coastal system: A case study of Jiaozhou Bay, China. *Ocean Dyn.* **2012**, *62*, 1443–1456. [CrossRef]
6. Kim, S.Y.; Cornuelle, B.D.; Terrill, E.J. Decomposing observations of high-frequency radar-derived surface currents by their forcing mechanisms: Locally wind-driven surface currents. *J. Geophys. Res. Earth Surf.* **2010**, *115*, C12046. [CrossRef]
7. Holloway, G. Systematic forcing of large-scale geophysical flows by eddy-topography interaction. *J. Fluid Mech.* **1987**, *184*, 463–476. [CrossRef]
8. Callies, U.; Gaslikova, L.; Kapitza, H.; Scharfe, M. German Bight residual current variability on a daily basis: Principal components of multi-decadal barotropic simulations. *Geo-Mar. Lett.* **2017**, *37*, 151–162. [CrossRef]
9. Cheng, P.; Valle-Levinson, A. Influence of Lateral Advection on Residual Currents in Microtidal Estuaries. *J. Phys. Oceanogr.* **2009**, *39*, 3177–3190. [CrossRef]
10. Dong, N.; Wang, G. Residual Current Analysis of the Yellow River Mouth Area in Bohai Gulf. *J. Oceanogr. Huanghai Bohai Seas* **1997**, *15*, 64–69.
11. Matte, P.; Secretan, Y.; Morin, J. Drivers of residual and tidal flow variability in the St. Lawrence fluvial estuary: Influence on tidal wave propagation. *Cont. Shelf Res.* **2019**, *174*, 158–173. [CrossRef]
12. Kilbourne, B.F. *On the Topic of Oceanic Variability near the Coriolis Frequency; Generation Mechanisms, Observations, and Implications for Interior Mixing*; Research Works Archive, University Libraries, University of Washington: Siettle, WA, USA, 2015; p. 150.
13. Bradbury, M.C.; Conley, D.C. Using Artificial Neural Networks for the Estimation of Subsurface Tidal Currents from High-Frequency Radar Surface Current Measurements. *Remote Sens.* **2021**, *13*, 3896. [CrossRef]
14. Poul, H.M.; Backhaus, J.; Dehghani, A.; Huebner, U. Effect of subseabed salt domes on Tidal Residual currents in the Persian Gulf. *J. Geophys. Res. Ocean.* **2016**, *121*, 3372–3380. [CrossRef]
15. Dobrynin, M.; Kleine, T.; Düsterhus, A.; Baehr, J. Skilful Seasonal Prediction of Ocean Surface Waves in the Atlantic Ocean. *Geophys. Res. Lett.* **2019**, *46*, 1731–1739. [CrossRef]
16. Gonzalez, P.L.M.; Brayshaw, D.J.; Zappa, G. The contribution of North Atlantic atmospheric circulation shifts to future wind speed projections for wind power over Europe. *Clim. Dyn.* **2019**, *53*, 4095–4113. [CrossRef]
17. Fernand, L.; Nolan, G.D.; Raine, R.; Chambers, C.E.; Dye, S.R.; White, M.; Brown, J. The Irish coastal current: A seasonal jet-like circulation. *Cont. Shelf Res.* **2006**, *26*, 1775–1793. [CrossRef]
18. Han, Q.; Gui, C.; Xu, J.; Lacidogna, G. A generalized method to predict the compressive strength of high-performance concrete by improved random forest algorithm. *Constr. Build. Mater.* **2019**, *226*, 734–742. [CrossRef]
19. Ren, L.; Nagle, D.; Hartnett, M.; Nash, S.J.E. The Effect of Wind Forcing on Modeling Coastal Circulation at a Marine Renewable Test Site. *Energies* **2017**, *10*, 2114. [CrossRef]
20. Gui, R.Z. Adaptively Selecting Working Frequency to Reduce Disturbances in High Frequency Radar. *Acta Phys. Pol. A* **2011**, *119*, 473–478. [CrossRef]
21. Basañez, A.; Pérez-Muñuzuri, V. HF Radars for Wave Energy Resource Assessment Offshore NW Spain. *Remote Sens.* **2021**, *13*, 2070. [CrossRef]
22. Saviano, S.; Esposito, G.; Di Lemma, R.; de Ruggiero, P.; Zambianchi, E.; Pierini, S.; Falco, P.; Buonocore, B.; Cianelli, D.; Uttieri, M. Wind Direction Data from a Coastal HF Radar System in the Gulf of Naples (Central Mediterranean Sea). *Remote Sens.* **2021**, *13*, 1333. [CrossRef]
23. Tseng, Y.-H.; Lu, C.-Y.; Zheng, Q.; Ho, C.-R. Characteristic Analysis of Sea Surface Currents around Taiwan Island from CODAR Observations. *Remote Sens.* **2021**, *13*, 3025. [CrossRef]
24. Cosoli, S.; Mazzoldi, A.; Gačić, M. Validation of Surface Current Measurements in the Northern Adriatic Sea from High-Frequency Radars. *J. Atmos. Ocean. Technol.* **2010**, *27*, 908–919. [CrossRef]
25. Chen, Y.-R.; Paduan, J.D.; Cook, M.S.; Chuang, L.Z.-H.; Chung, Y.-J. Observations of Surface Currents and Tidal Variability Off of Northeastern Taiwan from Shore-Based High Frequency Radar. *Remote Sens.* **2021**, *13*, 3438. [CrossRef]
26. An, Z. Study of Ocean Currents Detection with HF Ground Wave Over-the-Horizon Radar. Ph.D. Thesis, Xidian University, Xi'an, China, 2008.
27. Xiao, J. Research on Current Data Processing Method of High Frequency Surface Wave Radar. Master's Thesis, Wuhan University, Wuhan, China, 2017.
28. Silva, M.T.; Huang, W.; Gill, E.W. Bistatic High-Frequency Radar Cross-Section of the Ocean Surface with Arbitrary Wave Heights. *Remote Sens.* **2020**, *12*, 667. [CrossRef]
29. Novi, L.; Raffa, F.; Serafino, F. Comparison of Measured Surface Currents from High Frequency (HF) and X-Band Radar in a Marine Protected Coastal Area of the Ligurian Sea: Toward an Integrated Monitoring System. *Remote Sens.* **2020**, *12*, 3074. [CrossRef]
30. Lei, R.; Manman, W.; Huayang, C.; Zhan, H.; Qingshu, Y.; Hartnett, M. Characteristics of coastal currents based on High Frequency radar and ADCP observations in the Strait of Georgia. *IOP Conf. Ser. Earth Environ. Sci.* **2018**, *189*, 052042.

31. Shibendu, M.; Rajib, K.; Durbadal, M. Direct digital fractional-order Butterworth filter design using constrained optimization. *AEU Int. J. Electron. Commun.* **2021**, *128*, 153511.
32. Emery, W.J.; Thomson, R.E. *Data Analysis Methods in Physical Oceanography*, 2nd ed.; Elsevier Science: Amsterdam, The Netherlands, 2001.
33. Ma, J. Rotary spectrum estimation of ocean current vector time series and its application. *ACTA Oceanol. Sin.* **1987**, *4*, 510–518.
34. Chen, Y. Spatio-Temporal Characteristics and Influencing Factors of Current in Qinhuangdao Coastal Area. Master's Thesis, Shanghai Ocean University, Shanghai, China, 2019.
35. Mihanović, H.; Cosoli, S.; Vilibić, I.; Ivanković, D.; Dadić, V.; Gačić, M. Surface current patterns in the northern Adriatic extracted from high-frequency radar data using self-organizing map analysis. *J. Geophys. Res. Earth Surf.* **2011**, *116*. [CrossRef]
36. Wang, H.; Wu, L.; Chai, H.; Xiao, Y.; Hsu, H.; Wang, Y. Characteristics of Marine Gravity Anomaly Reference Maps and Accuracy Analysis of Gravity Matching-Aided Navigation. *Sensors* **2017**, *17*, 1851. [CrossRef]
37. Xing, C.; Zhao, Q.; Cao, X.; Yang, Y.; Song, L. Seasonal variation of the coastal currents in the Northern Bohai Strait. *Mar. Environ. Sci.* **2020**, *39*, 334–339.
38. Hickey, B.M.; Hamilton, P. A Spin-Up Model as a Diagnostic Tool for Interpretation of Current and Density Measurements on the Continental Shelf of the Pacific Northwest. *J. Phys. Oceanogr.* **1980**, *10*, 12–24. [CrossRef]